arXiv:2112.02180v1 [stat.CO] 3 Dec 2021

Generalized Transitional Markov Chain Monte Carlo Sampling Technique for Bayesian Inversion

Han Lu[a], Mohammad Khalil[b], Thomas Catanach[b], Jiefu Chen[a], Xuqing Wu[a], Xin Fu[a], Cosmin Safta[b], Yueqin Huang[c]

[a] *University of Houston, Houston, Texas 77204, USA*
[b] *Sandia National Laboratories, Livermore, California 94550, USA*
[c] *Cyentech Consulting LLC, Cypress, Texas 77429, USA*

Abstract

In the context of Bayesian inversion for scientific and engineering modeling, Markov chain Monte Carlo sampling strategies are the benchmark due to their flexibility and robustness in dealing with arbitrary posterior probability density functions (PDFs). However, these algorithms been shown to be inefficient when sampling from posterior distributions that are high-dimensional or exhibit multi-modality and/or strong parameter correlations. In such contexts, the sequential Monte Carlo technique of transitional Markov chain Monte Carlo (TMCMC) provides a more efficient alternative. Despite the recent applicability for Bayesian updating and model selection across a variety of disciplines, TMCMC may require a prohibitive number of tempering stages when the prior PDF is significantly different from the target posterior. Furthermore, the need to start with an initial set of samples from the prior distribution may present a challenge when dealing with implicit priors, e.g. based on feasible regions. Finally, TMCMC can not be used for inverse problems with improper prior PDFs that represent lack of prior knowledge on all or a subset of parameters. In this investigation, a generalization of TMCMC that alleviates such challenges and limitations is proposed, resulting in a tempering sampling strategy of enhanced robustness and computational efficiency. Convergence analysis of the proposed sequential Monte Carlo algorithm is presented, proving that the distance between the intermediate distributions and the target posterior distribution monotonically decreases as the algorithm proceeds. The enhanced efficiency associated with the pro-

Email address: mkhalil@sandia.gov (Mohammad Khalil)

posed generalization is highlighted through a series of test inverse problems and an engineering application in the oil and gas industry.

Keywords: Bayesian Updating, Inverse Problems, Markov chain Monte Carlo, Uncertainty Quantification, Importance Sampling, Logging-while-drilling, Electromagnetic data

---

1. Introduction

Bayesian inference, an application of Bayes' theorem for statistical inference, has been increasingly applied in many scientific and engineering disciplines. In such settings, Bayesian inference provides the means to update predictive models of the physical process of interest using available observations while accounting for uncertainties in the observations, model parameters and model structure. Among various Bayesian inference methods, Markov chain Monte Carlo (MCMC) sampling [1, 2] is the most popular method due to its reliability, generality, and ease of implementation [3]. However, traditional MCMC methods, such as Metropolis-Hastings (MH) [4], can be inefficient when the target posterior probability density function (PDF) is (a) high dimensional [5, 6, 7], (b) exhibits multi-modality [8], or (c) when the unknown variables are highly correlated [9] such that the posterior PDF approximates a low-dimensional manifold in parameter space. To alleviate such limitations, a variety of MCMC variants have been developed such as adaptive MCMC [10, 11], parallel tempered MCMC [12], and hybrid Monte Carlo [13]. In particular, the transitional MCMC (TMCMC) algorithm was first proposed for applications of Bayesian inference in structural dynamics and other engineering applications [14]. TMCMC, and associated extensions, are generally classified as Sequential Monte Carlo (SMC) methods which evolve populations of samples through a sequence of distributions [15, 16, 17, 18]. Instead of directly sampling from the target PDF, TMCMC generates samples from a series of intermediate PDFs that gradually evolve from the prior to the posterior distribution, and are focused on efficiently concentrating the samples in regions of parameter space with high probability mass according to the posterior distribution. At each iteration of TMCMC, the likelihood function can be independently evaluated across all samples, leading to naturally parallelizable sampling strategies as opposed to standard MCMC methods that evaluate the likelihood sequentially. The ability to sample from complex target PDFs in parallel has promoted TM-

CMC, and its modified versions, for use in estimating model parameters in many areas of application [19, 20, 21, 22, 23, 24, 25, 26, 27].

Parallel tempering (PT) [28, 29, 18, 30] is another approach that is similar to TMCMC in two aspects: (a) deal with a set of intermediate PDFs with associated tempering parameter and (b) provide means of achieving parallelism through multiple MCMC chains. However, the main difference between the two sets of algorithms relate to the means of achieving parallelism: TMCMC runs multiple MCMC chains for each stage (with an associated tempering parameter) whereas PT runs multiple chains, one for each tempering parameter value. In practice, one must start with a pre-specified temperature schedule for PT (in an offline phase) whereas TMCMC learns the optimal temperature schedule based on the target PDF of interest. Furthermore, unlike many MCMC algorithms, TMCMC does not normally suffer from burn-in, the generation of samples at the initial stages of an MCMC algorithm that are not distributed according to the target or stationary PDF. The samples that are generated during the burn-in phase are typically discarded, reducing the overall efficiency of MCMC. TMCMC does not normally have a burn-in period since the initial distribution is the prior PDF as opposed to an arbitrary distribution associated with initial sample generation for MCMC. Another important feature of TMCMC is that it provides an estimate of the Bayesian model evidence [31], an essential quantity in Bayesian model selection [32, 33] and model averaging [34, 35], at normally negligible additional cost.

In applications of TMCMC to Bayesian inference, the initial samples are drawn from the prior PDF which characterizes the initial knowledge, or lack thereof, of the parameter vector. Those samples are transitioned from one stage/intermediate PDF to the next using a combination of a sampling importance resampling [36] step and MCMC simulations, finally arriving at an ensemble that is distributed according to the posterior PDF. TMCMC has been shown to be effective in dealing with posterior PDFs that are high-dimensional, exhibit multi-modality and/or strong parameter correlations. This has prompted recent efforts towards the development of algorithms that are modifications of or related to TMCMC, such as algorithms that deal with "big data" [37, 38] and algorithms that couple TMCMC with more efficient MCMC samplers [39, 24]. Nonetheless, existing TMCMC algorithms still face computational and formulation issues that might limit their applicability in practical applications of Bayesian inference.

For a pre-specified sampling error budget, a prior PDF that is somewhat

"closer" to the posterior PDF often reduces the number of TMCMC tempering stages and the associated forward model simulations for likelihood evaluation. The opposite is also true in that a prior PDF that is too diffuse with respect to the posterior would place prohibitive computational costs due to increasing number of stages to achieve the same level of sampling error. In Bayesian calibration tasks, modelers might assign improper priors to parameters to represent the lack of knowledge. *TMCMC can not be applied to Bayesian calibration tasks involving such uninformative improper prior PDFs due to the inability to provide an initial set of samples to TMCMC*. There are also scenarios in which the prior knowledge on unknown parameters is in the form of constraints that are strongly tied to the physical laws associated with the system being modeled. In such settings, the prior PDF takes the form of a uniform density on the feasible region being the set of all possible points in parameter space that satisfy such constraints. In such scenarios, direct Monte Carlo sampling of such "implicit" prior PDFs becomes challenging, especially as the number of constraints, the degree of constraint non-linearities, and/or the dimensionality (i.e. number of unknown parameters) increase. Although sampling from a feasible set may be achieved using importance sampling (IS), sampling importance resampling as well as rejection sampling [40], there might be situations when the feasible set is unbounded, leading again to improper prior PDFs. The modeler might feel compelled to further constraint the parameters to arrive at a proper prior PDF in order to use TMCMC, but such constraints might strongly influence the posterior PDFs and subsequent model predictions.

The SMC approach presented herein is a generalization of TMCMC that allows the algorithm to start with an arbitrary initial state, an importance PDF, instead of the traditional prior PDF as is the case for classical variants of TMCMC. The proposed generalized TMCMC (GTMCMC) technique is a tempering algorithm [18] in that it generally allows both cooling and heating of the solution depending on the choice of importance PDF with respect to the target posterior PDF. The number of TMCMC stages, and associated forward model simulations for likelihood evaluation, may be dramatically reduced when the importance distribution is chosen judiciously to more closely resemble the target posterior PDF than does the prior PDF. Furthermore, the importance distribution may be chosen to be one that is easy to generate samples from in comparison to prior PDFs that might be based on feasible sets. The ability to start with samples from an arbitrary importance PDF would also extend the applicability of the proposed TMCMC algorithm to situations

involving improper prior PDFs, a major limitation of traditional TMCMC algorithms. It is also important to note that when the importance PDF is chosen as the prior PDF, the proposed algorithm behaves exactly as the traditional TMCMC algorithm. Therefore, this approach can be considered as a generalization of the original TMCMC sampling technique. The proposed GTMCMC algorithm addresses several challenges/inefficiencies that standard TMCMC suffers from towards providing a more robust and efficient tempering sampling strategy, namely:

1. Bayesian inference problems involving improper priors which prevent the use of TMCMC
2. Difficult to sample priors, including implicit priors, where the prior is not explicitly defined as a function of parameters but as a function of some other quantifies of interests and therefore can typically only be sampled through rejection sampling and other similar approaches.
3. Solving sequences of related Bayesian inference problems where parameter posterior PDFs are "close" to previously obtained solutions of similar inverse problems (in contrast to prior PDFs). This concept is similar to training tasks in machine learning whereby transfer learning [41] is used.

The remainder of this paper is organized as follows. Section 2 serves as an introduction into Bayesian inference for scientific and engineering system. Section 3 overviews TMCMC sampling for Bayesian inversion and Section 4 presents the proposed GTMCMC sampling algorithm. In Section 5, we demonstrate the advantages of the new algorithm over the standard TMCMC through several comparative numerical investigations. In Section 6, we apply the proposed algorithm on an engineering application in the oil and gas industry: the inversion of the ultra-deep directional resistivity data obtained from the logging-while-drilling tool. Finally, we provide concluding remarks and observations regarding the proposed algorithm in Section 7.

2. Bayesian Inference

Given a forward model f, unknown parameter vector $\boldsymbol{\theta} \in \mathbb{R}^{N_\theta}$, and experimental parameter vector $\boldsymbol{x}$, the noisy observation vector $\boldsymbol{d}_j \in \mathbb{R}^{N_d}$ may be given by

$$\boldsymbol{d}_j = f(\boldsymbol{\theta}, \boldsymbol{x}) + \epsilon_j \ , \tag{1}$$

in which $\boldsymbol{\epsilon_j}$ is a specific realization of the measurement error vector $\epsilon \in \mathbb{R}^{N_\epsilon}$. Given a set of noisy measurements $\boldsymbol{D} = \{\boldsymbol{d}_1, \ldots, \boldsymbol{d}_N\}$, associated with pre-specified experimental parameter vector realizations $\boldsymbol{X} = \{\boldsymbol{x}_1, \ldots, \boldsymbol{x}_N\}$ the inverse problem associated with inferring the unknown (or weakly known) parameter vector $\boldsymbol{\theta}$ may be solved using Bayesian inference [42], with Bayes' law providing the solution in the form of a joint PDF given by

$$p(\boldsymbol{\theta}|\boldsymbol{D}) \propto p(\boldsymbol{D}|\boldsymbol{\theta})p(\boldsymbol{\theta}) \ , \tag{2}$$

where $p(\boldsymbol{\theta}|\boldsymbol{D})$ represents posterior PDF, $p(\boldsymbol{D}|\boldsymbol{\theta})$ is the likelihood of the data $\boldsymbol{D}$ for a given realization of the parameter vector $\boldsymbol{\theta}$, and $p(\boldsymbol{\theta})$ is the prior PDF that encapsulates any knowledge about the parameter vector prior to assimilating the available data.

Under specific circumstances in which the forward model is linear in both the unknown parameter vector θ and the measurement error vector, and with a multivariate Gaussian measurement error vector and Gaussian prior PDF, the posterior PDF is exactly Gaussian. Generally, the posterior is not Gaussian and the analytical solution of the posterior distribution is intractable. In such situations, a popular approach is to apply MCMC sampling to draws a series of samples from $p(\boldsymbol{\theta}|\boldsymbol{D})$ by constructing a Markov chain that has the target posterior as its equilibrium/stationary distribution [10, 11].

In practical scenarios, many samples (1×10^6 or more) are needed to effectively explore the parameter space in regions associated with high probabilities for subsequent predictive tasks. This issue is exacerbated by the fact that MCMC methods produce correlated, rather than independent, samples, with an associated correlation length that tends to increase with increasing problem dimensionality. Many efforts have focused designing more effective proposal distributions that aim to decrease the correlation length associated with the samples. However, to date, optimal proposal distributions are only available in simplistic settings [7, 43]. Therefore, it is necessary to explore more efficient sampling methods for such problems. Furthermore, MCMC relies on sequential evaluation of the posterior PDF and associated likelihood function through forward model simulations due to the reliance on a Markov chain for sampling. This limits the applicability of MCMC towards solving inverse problems involving computationally intensive forward model simulations as it limits the use of high performance computing to evaluate samples in parallel.

3. Transitional Markov chain Monte Carlo

While MCMC draws samples from the target PDF in a sequential manner, TMCMC generates samples from a series of intermediate PDFs that gradually evolve from the prior to the posterior (target) distribution, and are focused on efficiently concentrating the samples in regions of parameter space with high probability mass according to the posterior distribution. At each iteration of TMCMC, the likelihood function can be independently evaluated across all samples, leading to naturally parallel sampling strategies as opposed to sequential MCMC methods. Various investigations have demonstrated the enhanced efficiency of TMCMC, in comparison to MCMC, when generating samples from complex target posterior PDFs [19, 20, 21, 22, 23, 24, 25, 26]. Additionally, TMCMC provides an estimate for the Bayesian model evidence [31] with minimal additional cost without further model (likelihood) evaluations.

As previously mentioned, TMCMC constructs and samples from a series of intermediate PDFs. Consider the following intermediate PDFs

$$p_j(\boldsymbol{\theta}) \propto p(\boldsymbol{D}|\boldsymbol{\theta})^{\beta_j} p(\boldsymbol{\theta}) \ , \tag{3}$$

with $j = 0, \ldots, m$ and $0 = \beta_0 < \beta_1 < \ldots < \beta_m = 1$, where index j denotes the TMCMC stage number associated with a specific tempering parameter β_j. The intermediate PDFs p_j transition from the prior PDF $p(\boldsymbol{\theta})$ towards the posterior PDF $p(\boldsymbol{\theta}|\boldsymbol{D})$. Though the topology change from $p(\boldsymbol{\theta})$ to $p(\boldsymbol{\theta}|\boldsymbol{D})$ can be dramatic, the change between two subsequent intermediate PDFs can be gradual through a judicious selection of β_j, thus making it possible to efficiently "nudge" or transition the samples from one stage to the next. We summarize the TMCMC algorithm in Algorithm 1.

Algorithm 1 Transitional Markov chain Monte Carlo

Input: Prior PDF, $p(\boldsymbol{\theta})$; Likelihood function, $p(\boldsymbol{D}|\boldsymbol{\theta})$; Number of samples, n; Target coefficient of variation, CoV, of the weights; Prescribed scaling factor for MCMC proposal covariance matrix, γ; MCMC chain length, N

Result: Samples from posterior PDF, $\{\boldsymbol{\theta}_1, \ldots, \boldsymbol{\theta}_n\}$ & Model evidence estimate, S

$\beta_0 \leftarrow 0 \quad k \leftarrow 0$

Generate samples $\{\boldsymbol{\theta}_1^{(0)}, \ldots, \boldsymbol{\theta}_n^{(0)}\}$ from $p(\boldsymbol{\theta})$

while $\beta_k < 1$ **do**

Compute likelihood of ensemble of realizations $p(\boldsymbol{D}|\boldsymbol{\theta}_l^{(k)})$, $l = 1, \ldots, n$

Compute the weight of each sample $w(\boldsymbol{\theta}_l^{(k)}) = p(\boldsymbol{D}|\boldsymbol{\theta}_l^{(k)})^{\beta_{k+1}-\beta_k}$, with β_{k+1} chosen such that coefficient of variation of those weights is equal to the target CoV

Compute contribution to model evidence, $S_k = \frac{1}{n}\sum_{l=1}^{n} w(\boldsymbol{\theta}_l^{(k)})$

Compute the ensemble covariance matrix to be used in MCMC simulations:

$$\tilde{w}(\boldsymbol{\theta}_l^{(k)}) = \frac{w(\boldsymbol{\theta}_l^{(k)})}{\sum_{l=1}^{n} w(\boldsymbol{\theta}_l^{(k)})} \qquad \overline{\boldsymbol{\theta}}^{(k)} = \sum_{k=1}^{n} \boldsymbol{\theta}_l^{(k)} \tilde{w}(\boldsymbol{\theta}_l^{(k)})$$

$$\boldsymbol{\Sigma}^{(k)} = \gamma^2 \sum_{k=1}^{n} \tilde{w}(\boldsymbol{\theta}_l^{(k)})(\boldsymbol{\theta}_l^{(k)} - \overline{\boldsymbol{\theta}}^{(k)})(\boldsymbol{\theta}_l^{(k)} - \overline{\boldsymbol{\theta}}^{(k)})^T$$

Resampling: Generate n random samples, $\{\tilde{\boldsymbol{\theta}}_1^{(k)}, \ldots, \tilde{\boldsymbol{\theta}}_n^{(k)}\}$, from the current ensemble $\{\boldsymbol{\theta}_1^{(k)}, \ldots, \boldsymbol{\theta}_n^{(k)}\}$ with corresponding probabilities $\tilde{w}(\boldsymbol{\theta}_l^{(k)})$

for $l \leftarrow 1$ **to** n **do**

$\boldsymbol{x}_0 \leftarrow \tilde{\boldsymbol{\theta}}_l^{(k)}$

for $i \leftarrow 0$ **to** $N-1$ **do**

Generate $\hat{\boldsymbol{x}}$ from Gaussian proposal $\mathcal{N}(\boldsymbol{x}_i, \boldsymbol{\Sigma}^{(k)})$

Compute acceptance probability, $\alpha = \min\{1, \frac{p(\hat{\boldsymbol{x}})p(\boldsymbol{D}|\hat{\boldsymbol{x}})^{\beta_{k+1}}}{p(\boldsymbol{x}_i)p(\boldsymbol{D}|\boldsymbol{x}_i)^{\beta_{k+1}}}\}$

Generate u from from the continuous uniform distribution on the interval $[0, 1]$

if $u < \alpha$ **then**

$\boldsymbol{x}_{i+1} = \hat{\boldsymbol{x}}$

else

$\boldsymbol{x}_{i+1} = \boldsymbol{x}_i$

end if

end for

$\boldsymbol{\theta}_l^{(k+1)} \leftarrow \boldsymbol{x}_N$

end for

$k \leftarrow k + 1$

end while

$m \leftarrow k - 1$

Compute model evidence estimate, $S \leftarrow \prod_{l=0}^{m} S_l$

for $l \leftarrow 1$ **to** n **do** $\boldsymbol{\theta}_l = \boldsymbol{\theta}_l^{(m)}$

For our implementation of TMCMC and the proposed GTMCMC (described next), the coefficient of variation[1] of the weights at any stage is a measure of the discrepancy between the intermediate PDFs associated with successive tempering parameter values, β_k and β_{k+1}. Therefore, in order to control the rate of change in the intermediate PDFs, β_{k+1} is chosen so that the resulting coefficient of variation of the weights is equal to some prespecified value, CoV. This is essentially a root-finding problem and one could rely on the bisection method to determine β_{k+1}. As for the MCMC proposal covariance scaling parameter, a value of $\gamma^2 = 0.04$ is suggested in Ref. [14]. However, this is likely to be sub-optimal depending on the problem involved, particularly when parameters are highly correlated. In this work, we use an adaptive formulation for γ^2, first proposed in Ref. [44], based on a feedback control strategy in order to produce a target MCMC acceptance rate of 0.234. Though only one MCMC step, $N = 1$, is taken per sample for all the results presented in Sections 5 and 6, the algorithm allows for an arbitrary length for the chains in each stage in order to achieve convergence. TMCMC allows for a straightforward parallelization over the number of samples n during each stage. During each stage, each sample will be advanced a number of MCMC iterations $N \geq 1$, and the sampling progresses in m stages, resulting in a total of $n \times N \times m$ model evaluations. The n model evaluations, with n typically 10^3 to 10^4, can be performed in parallel at each stage and MCMC iteration, while the $N \times m$ model evaluations within chain and across stages are sequential in nature, with $N \approx 1$ to 10 and $m \approx 10$ to 100.

4. Generalization of Transitional Markov chain Monte Carlo

TMCMC is a sampling algorithm that relies on the concept of "transitioning" an ensemble of realizations from an initial state, i.e. distributed according to a prior PDF in a Bayesian setting, to a final state, i.e. a posterior PDF. From an uncertainty point of view, the transition PDFs (from prior to posterior) are often associated with monotonically decreasing uncertainty. Therefore, TMCMC can be classified as an annealing algorithm [45, 46] that starts with an initial "hot" state (with greater uncertainty) and ends at a final "cold" solution (lower uncertainty). The samples are transitioned from one state to the next using sampling importance resampling

[1] taken to be the sample standard deviation normalized by the sample mean

(SIR) [40], whereby the resampling is achieved via multiple MCMC chains (one per unique sample) that aim to infuse diversity in the samples (ensuring that the ensemble is distributed according to the intermediate PDF associated with that particular stage).

Herein, we will present an extension, or generalization, of TMCMC that allows the algorithm to start with an arbitrary initial state, i.e. an importance PDF, $q(\boldsymbol{\theta})$, instead of the traditional prior PDF, $p(\boldsymbol{\theta})$. In some sense, the proposed technique is a tempering algorithm [18], rather than a stricter classification as an annealing algorithm, in that it generally allows both cooling and heating of the solution depending on the choice of $q(\boldsymbol{\theta})$. In this generalized framework, the modeler has the option of starting with an importance PDF exhibiting lower associated uncertainty in contrast to the posterior and let the algorithm transition from this "colder" state to the target posterior. This might be helpful in practice when faced with implicit priors, for example, in which starting with a "warmer" state might results with an initial ensemble with lots of samples in the infeasible region of parameter space (with zero associated prior probability). Furthermore, in the situation that the proposal PDF is chosen to be the prior one, the algorithm reverts back to TMCMC as will be described next.

Starting with Bayes' rule, we leverage the concept of importance sampling to introduce an importance PDF $q\left(\boldsymbol{\theta}\right)$ that we can easily sample from:

$$p\left(\boldsymbol{\theta}|\boldsymbol{D}\right) \propto q\left(\boldsymbol{\theta}\right) \frac{p\left(\boldsymbol{\theta}\right) p\left(\boldsymbol{D}|\boldsymbol{\theta}\right)}{q\left(\boldsymbol{\theta}\right)} \tag{4}$$

This importance PDF will be used to initialize the proposed generalized TMCMC (GTMCMC) algorithm as follows. Similar to the approach first proposed by Neal [47] and subsequently adopted for TMCMC [9, 14], we will sample from a series of 'transitional' or intermediate PDFs that are controlled by a tempering (or annealing) parameter, β_m, as in

$$\begin{aligned} p_j(\boldsymbol{\theta}) &\propto \left(\frac{p\left(\boldsymbol{\theta}\right) p\left(\boldsymbol{D}|\boldsymbol{\theta}\right)}{q\left(\boldsymbol{\theta}\right)}\right)^{\beta_j} q(\boldsymbol{\theta}) \\ &= \left(p\left(\boldsymbol{\theta}\right) p\left(\boldsymbol{D}|\boldsymbol{\theta}\right)\right)^{\beta_j} q(\boldsymbol{\theta})^{1-\beta_j} \ , \end{aligned} \tag{5}$$

with $j = 0, \ldots, m$ and $0 = \beta_0 < \beta_1 < \ldots < \beta_m = 1$. As β increases, the intermediate distribution $p_j(\boldsymbol{\theta})$ monotonically gets closer to the posterior in the KL-Divergence, see Appendix A. As with traditional TMCMC, β_j may be adaptively tuned using the coefficient of variation of the sample weights.

The proof in Appendix B shows that the CoV of the sample population is monotonically increasing so β_j may be found efficiently using a variety of optimization methods.

The novelty of the proposed strategy lies in utilizing an importance distribution in the context of solving a Bayesian inverse problem, resulting in a new sequential monte Carlo sampler. Of most significant consequence is the potential to dramatically reduce the number of TMCMC stages, m, if an importance distribution, $q(\boldsymbol{\theta})$, resembling the posterior PDF, $p(\boldsymbol{\theta}|\boldsymbol{D})$, is used. In practice, the importance distribution is one that is easy to generate samples from, such as a multi-variate Gaussian. Although importance sampling can achieve remarkable results in drastically reducing the number of TMCMC stages, this can only be achieved when that distribution is chosen judiciously for each target posterior PDF. This will be demonstrated for an application of relevance to the oil and gas industry, whereby the proposed methodology significantly reduces the number of stages m required in solving sequences of related Bayesian inference problems. More generally, the freedom to chose the initial density alleviates the limitation that TMCMC encounters when dealing with improper or complex prior PDFs that are difficult to sample from (the original TMCMC algorithm starts with initial samples that are obtained from Monte Carlo simulation of the pre-specified prior distribution). Note that if the importance density $q(\boldsymbol{\theta})$ is chosen as the prior PDF $p(\boldsymbol{\theta})$, then one reverts back to the standard TMCMC algorithm with the same intermediate PDFs. Therefore, this approach can be considered as a generalization of the original TMCMC sampling technique. The algorithm is summarized below:

As was mentioned previously for TMCMC, at any stage β_{k+1} is chosen so that the resulting coefficient of variation of the weights is equal to some pre-specified value, CoV, which again could be obtained through the bisector method or any other appropriate root-finding method. Similar to our implementation of standard TMCMC, we rely on an adaptive formulation for determining γ^2 in order to produce an optimal MCMC acceptance (see [44] for more details). It is important to note that the GTMCMC algorithm as presented relies on the Metropolis Hastings MCMC at every stage, but that can be replaced by a more efficient MCMC sampler for a given inverse problem.

Algorithm 2 Generalized Transitional Markov chain Monte Carlo

Input: Prior PDF, $p(\boldsymbol{\theta})$; Likelihood function, $p(\boldsymbol{D}|\boldsymbol{\theta})$; Importance PDF, $q(\boldsymbol{\theta})$; Number of samples, n; Target coefficient of variation, COV; Prescribed scaling factor for MCMC proposal covariance matrix, γ; MCMC chain length, N

Result: Samples from posterior PDF, $\{\boldsymbol{\theta}_1, \ldots, \boldsymbol{\theta}_n\}$ & Model evidence estimate, S

$\beta_0 \leftarrow 0 \quad k \leftarrow 0$

Generate samples $\{\boldsymbol{\theta}_1^{(0)}, \ldots, \boldsymbol{\theta}_n^{(0)}\}$ from $q(\boldsymbol{\theta})$

while $\beta_k < 1$ **do**

Compute likelihood of ensemble of realizations $p(\boldsymbol{D}|\boldsymbol{\theta}_l^{(k)})$, $l = 1, \ldots, n$

Compute the weight of each sample $w(\boldsymbol{\theta}_l^{(k)}) = \left(p\left(\boldsymbol{\theta}_l^{(k)}\right) p\left(\boldsymbol{D}|\boldsymbol{\theta}_l^{(k)}\right)\right)^{\beta_{k+1}-\beta_k} q(\boldsymbol{\theta}_l^{(k)})^{\beta_k-\beta_{k+1}}$, with β_{k+1} chosen such that coefficient of variation of those weights is equal to the target COV

Compute contribution to model evidence, $S_k = \frac{1}{n}\sum_{l=1}^{n} w(\boldsymbol{\theta}_l^{(k)})$

Compute the ensemble covariance matrix to be used in MCMC simulations:

$$\tilde{w}(\boldsymbol{\theta}_l^{(k)}) = \frac{w(\boldsymbol{\theta}_l^{(k)})}{\sum_{l=1}^{n} w(\boldsymbol{\theta}_l^{(k)})} \qquad \overline{\boldsymbol{\theta}}^{(k)} = \sum_{k=1}^{n} \boldsymbol{\theta}_l^{(k)} \tilde{w}(\boldsymbol{\theta}_l^{(k)})$$

$$\boldsymbol{\Sigma}^{(k)} = \gamma^2 \sum_{k=1}^{n} \tilde{w}(\boldsymbol{\theta}_l^{(k)})(\boldsymbol{\theta}_l^{(k)} - \overline{\boldsymbol{\theta}}^{(k)})(\boldsymbol{\theta}_l^{(k)} - \overline{\boldsymbol{\theta}}^{(k)})^T$$

Resampling: Generate n random samples, $\{\tilde{\boldsymbol{\theta}}_1^{(k)}, \ldots, \tilde{\boldsymbol{\theta}}_n^{(k)}\}$, from the current ensemble $\{\boldsymbol{\theta}_1^{(k)}, \ldots, \boldsymbol{\theta}_n^{(k)}\}$ with corresponding probabilities $\tilde{w}(\boldsymbol{\theta}_l^{(k)})$

for $l \leftarrow 1$ **to** n **do**

$\boldsymbol{x}_0 \leftarrow \tilde{\boldsymbol{\theta}}_l^{(k)}$

for $i \leftarrow 0$ **to** $N-1$ **do**

Generate $\hat{\boldsymbol{x}}$ from Gaussian proposal $\mathcal{N}(\boldsymbol{i}_k, \boldsymbol{\Sigma}^{(k)})$

Compute acceptance probability, $\alpha = \min\left\{1, \frac{(p(\hat{\boldsymbol{x}})p(\boldsymbol{D}|\hat{\boldsymbol{x}}))^{\beta_{k+1}} q(\hat{\boldsymbol{x}})^{1-\beta_{k+1}}}{(p(\boldsymbol{x}_i)p(\boldsymbol{D}|\boldsymbol{x}_i))^{\beta_{k+1}} q(\boldsymbol{x}_i)^{1-\beta_{k+1}}}\right\}$

Generate u from from the continuous uniform distribution on the interval $[0, 1]$

if $u < \alpha$ **then**

$\boldsymbol{x}_{i+1} = \hat{\boldsymbol{x}}$

else

$\boldsymbol{x}_{i+1} = \boldsymbol{x}_i$

end if

end for

$\boldsymbol{\theta}_l^{(k+1)} \leftarrow \boldsymbol{x}_N$

end for

$k \leftarrow k + 1$

end while

$m \leftarrow k - 1$

Compute model evidence estimate, $S \leftarrow \prod_{l=0}^{m} S_l$

for $l \leftarrow 1$ **to** n **do** $\boldsymbol{\theta}_l = \boldsymbol{\theta}_l^{(m)}$

5. Numerical Tests

In this section, we will demonstrate the advantages of the GTMCMC algorithm over the TMCMC algorithm for a series of canonical test problems. In section 5.1, we generate samples from a 4-dimensional PDF using the TMCMC and the GTMCMC algorithm with different importance distributions and compare their errors in the mean prediction and the model evidence. In section 5.2, we perform scalability studies on a series of inverse problems of dimensionalities ranging from 1 through 8. In section 5.3, we evaluate the performance of the GTMCMC algorithm in estimating the model evidence with associated bi-modal posterior distributions. In section 5.4, we examine the performance of the proposed algorithm in sampling a strongly non-Gaussian posterior density with an associated negative log-likelihood Rosenbrock function.

5.1. Test 1: 4D Gaussian Prior and Likelihood

We first show the impact of using different importance distributions for the GTMCMC algorithm by solving a Bayesian inference problem with 4-dimensional (4D) standard Normal likelihood function. The prior distribution is a 4D tensor product of 1D Gaussian distributions all with mean and standard deviation of $(\mu, \sigma) = (1, 5)$, resulting in a Gaussian posterior distribution with associated mean of $1/26$ and variance of $25/26$ for each parameter. The mean of the importance PDF for the GTMCMC algorithm is fixed to 1 in all dimensions while the variance takes the values 0.6^2, 1^2, 3^2, and 5^2, independently for each dimension. Note that the last value for the variance coincides with that of the prior PDF, allowing us to also investigate the performance of the TMCMC algorithm. We also setup a test case with an importance PDF equal to the posterior distribution. We run the algorithm for each importance distribution with the hyper-parameter CoV varying from 0.1 to 1.

For the following set of results, GTMCMC is executed 1000 times to extract the average performance of this stochastic sampling algorithm. The number of samples per stage is fixed to 5×10^3 for all tests. Figure 1 shows the average number of stages used by the algorithm for each configuration across the 1000 repeated runs. The coefficient of variation, CoV, controls the evolution of tempering parameter β. A smaller CoV induces more transition stages to reach $\beta = 1$ and yields a more accurate result. We observe a near linear decrease in the number of TMCMC stages as we increase the allowable

coefficient of variation. In the case that the importance distribution is chosen to be the posterior distribution (available analytically for this problem), the GTMCMC algorithm converges in one step independent of the CoV value as expected since the initial set of samples are already drawn according to the target posterior. For the case in which the importance distribution is chosen to be the prior distribution, the GTMCMC algorithm reverts back to TMCMC, requiring a larger number of intermediate PDFs (and stages) to reach convergence in comparison to more compact importance distributions.

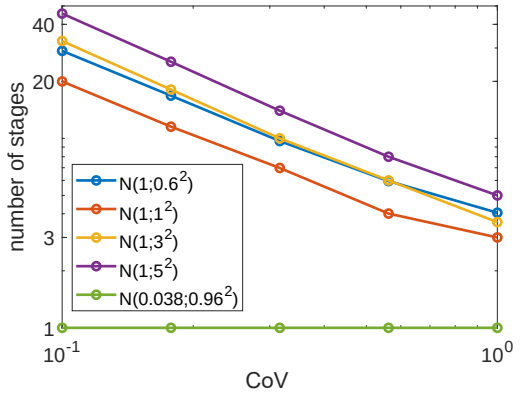
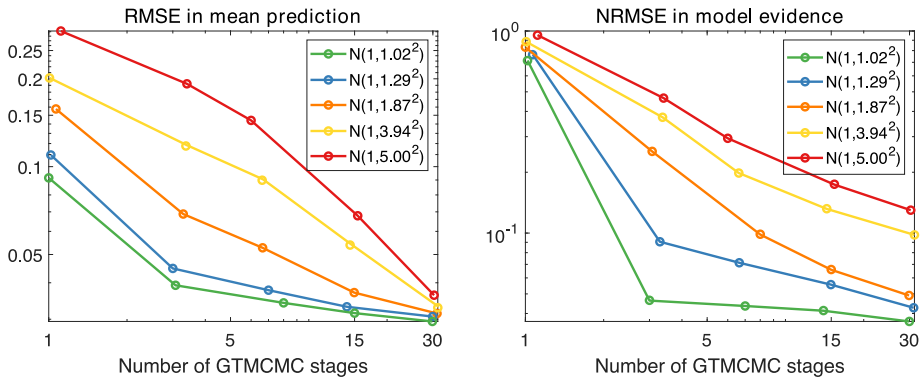


Figure 1: The average number of GTMCMC stages vs. CoV for different importance distributions

Next, the effect of importance distribution variance on the performance of GTMCMC is examined. For a fair comparison, the CoV is adjusted to ensure that the algorithm takes a target number of stages. The number of samples in each stage is 5×10^3 and again the algorithm is run 1000 times for each test. Figure 2 compares the root-mean-square-error (RMSE) in the posterior mean estimate and the normalized[2] RMSE (NRMSE) in the model evidence estimate obtained using the various importance distributions.

For all experiments, both the posterior mean estimates and the evidence estimates increase in accuracy as the number of stages increases (controlled via smaller CoV values). The errors associated with the standard TMCMC algorithm (red curves) indicate a diminished performance in comparison to GTMCMC relying on importance PDFs with lower associated variance than

[2]Normalization is achieved with respect to the corresponding analytical values of the model evidence.



(a) (b)

Figure 2: The error in estimating the posterior parameter mean and model evidence using GTMCMC versus the number of stages allowed: (a) RMSE in the posterior mean parameter estimates and (b) NRMSE in the evidence estimates. The curve labels refer the importance marginal distribution for each parameter.

the prior PDF.

These results suggest that given a computational budget based on the number of stages, the GTMCMC algorithm provides estimates of greater accuracy with a choice for importance distribution that is "closer" to the target posterior. Furthermore, the rate of decrease in the errors is greater for GTMCMC with certain importance distributions. Therefore, a judiciously chosen importance distribution can potentially result in computational savings for a given error budget associated with a threshold error. It is important to note that an importance distribution with greater uncertainty than that associated with the prior PDF may diminish the performance of GTMCMC in comparison to standard TMCMC .

The error in the model evidence estimates, shown in Figure 2(b), exhibits similar trends as those in the posterior mean estimates. For one allowable stage, all importance distributions result in similar NRMSE values. For greater number of stages examined, GTMCMC outperforms TMCMC in reducing the NRMSE in model evidence estimates for the importance distributions investigated

These observations suggest, as expected, that an importance PDF that is "closer" to the target posterior provides more precise estimates of the posterior mean and model evidence. They also suggest that in practice it

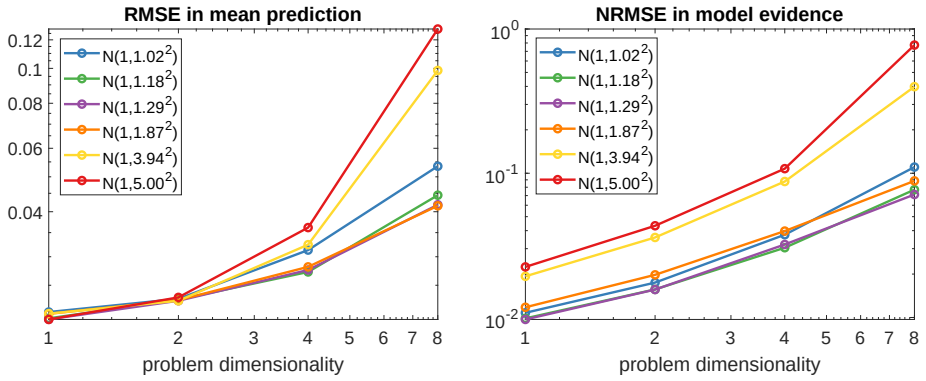
might be deemed worthwhile to focus on obtaining an "optimal" choice for the importance PDF, one that minimizes the error given a computational budget (number of allowable stages). This aspect is beyond the scope of this investigation.

5.2. Test 2: Performance with increased dimensionality

For the following investigation, the number of TMCMC stages is fixed to 20 in order to isolate the effect of the problem dimensionality (number of parameters to be inferred) in estimating the posterior parameter mean and model evidence. The same set of importance distributions are employed as in the previous subsection. The likelihood is a tensor product of one-dimensional standard Normal PDFs with problem dimensionality increasing from 1 to 8. The prior distribution for all experiments is a tensor product of one-dimensional Gaussians $\mathbf{N}(1, 5^2)$, resulting in a marginal posterior distribution of $\mathbf{N}(0.0385, 0.9625^2)$ for all parameters. The number of samples used for GTMCMC is fixed at 5×10^3. Error statistics are based on 2×10^3 repeated runs. Figure 3 shows the error in the posterior mean and model evidence estimates for different problem dimensionalities. It is obvious that the error in the posterior mean and the evidence estimates increase with the problem dimensionality, as expected (with a fixed number of samples and CoV). For problem dimensionalities greater than one, GTMCMC outperforms TMCMC for all chosen importance PDFs with smaller associated estimation errors than those obtained with TMCMC (GTMCMC with an importance distribution equal to the prior).

5.3. Test 3: Bi-modal Gaussian Posterior

In this subsection, we evaluate the performance of the GTMCMC algorithm for sampling a canonical 2D bi-modal posterior distribution. The likelihood is constructed as a weighted sum of two Gaussian distributions with parameters shown in Table 1, where $\mathbf{I}_n$ represents the n-D identity matrix. With a multi-variate normal prior distribution centered at $((0, 0)$ and diagonal covariance matrix $10^2 \times \mathbf{I}_2$, the posterior distribution is computed analytically with parameters given in Table 1. We run the GTMCMC algorithm with Gaussian importance distributions with several sets of parameter values. The posterior modes and selected importance means are shown in Figure 4. We set the covariance matrix to $10^2 \times \mathbf{I}_2$ for all mean values, and the test with the mean value of $(0, 0)$ represents the standard TMCMC algorithm. We adjust the CoV hyper-parameter to make the algorithm converge



(a) (b)

Figure 3: (a). The RMSE in the mean prediction and (b) The NRMSE in the evidence estimation when increasing problem dimensionality.

in 5, 10, 20, and 30 stages, respectively. Each configuration is simulated 10^4 times, and each run uses 10^4 samples.

Table 1: The likelihood and posterior parameters.

		center	cov. matrix	weight
Likelihood	Peak 1	(10, 0)	$\mathbf{I}_2$	25%
	Peak 2	(0, 10)	$\mathbf{I}_2$	75%
Posterior	Peak 1	(9.9, 0)	$0.99 \times \mathbf{I}_2$	25%
	Peak 2	(0, 9.9)	$0.99 \times \mathbf{I}_2$	75%

Figure 5 shows the error in evidence estimation. Similar to results shown in Figure 2(b), as more GTMCMC stages are included, the error in the model evidence decreases. Meanwhile, GTMCMC with importance PDFs centered at $(5, 5)$ and $(2, 8)$ always produce smaller error than the standard TMCMC algorithm (the red curve).

5.4. Test4: 3D Rosenbrock Posterior

In this subsection, we monitor the evolution of samples from the GTMCMC algorithm. The log-likelihood of the tested problem is defined is as follows

$$\log(p(d|x,y,z)) \propto -(100\times(y-x^2)^2+(1-x)^2+100\times(z-y^2)^2+(1-y)^2) \quad (6)$$

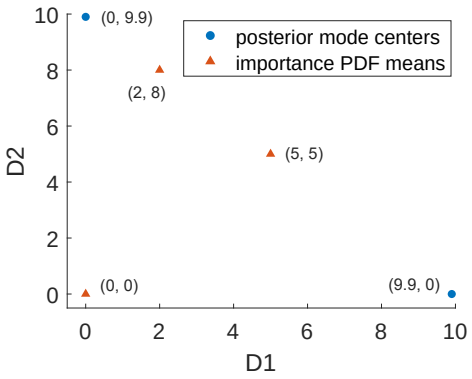


Figure 4: The centers of two posterior modes and selected importance distribution means.

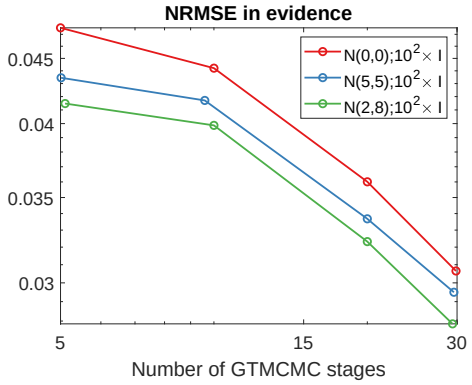


Figure 5: The NRMSE in the model evidence estimation.

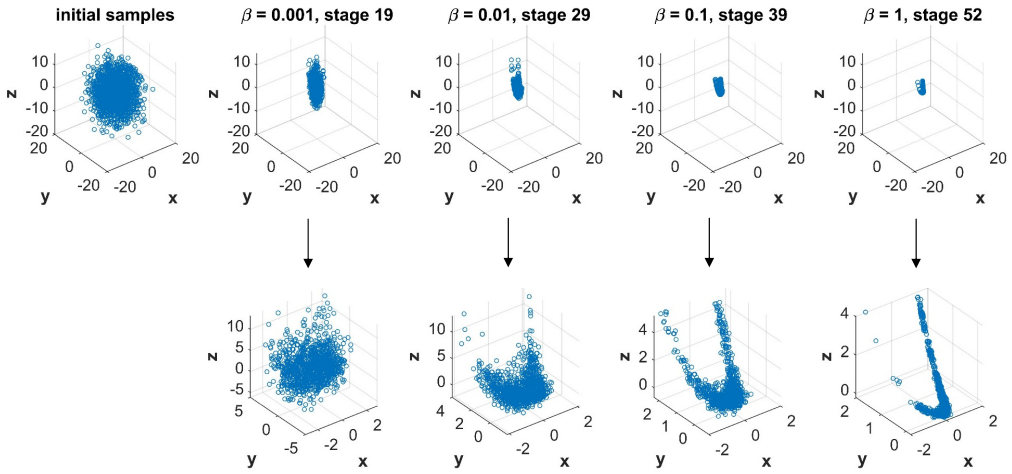
which is a 3D extension of the Rosenbrock function with variables x, y, and z. The maximum likelihood is inside a long, narrow, parabolic shaped valley in the 3D space. We set the prior distribution to be $\mathrm{N}((0,0,0); 5^2 \times \mathbf{I}_3)$. For the GTMCMC algorithm, we choose the importance distribution to be $\mathrm{N}((1,1,1); 2^2 \times \mathbf{I}_3)$ which is more informative than the prior distribution. We run the standard TMCMC and the GTMCMC algorithms for this problem with 2×10^3 samples and CoV $= 0.2$ for both. It takes 52 stages for TMCMC to transition from prior to posterior while for GTMCMC the number of stages is 39. Figure 6 shows 3D scatter plots of samples from different stages that correspond to select β values. The bottom rows of Figures 6(a) and 6(b), respectively, show zoomed-in regions where samples are concentrated. The

initial samples in the GTMCMC algorithm are more concentrated since the importance distribution of the algorithm has a smaller variance than the prior distribution. As a result, the GTMCMC algorithm takes less stages to converge compared to the standard TMCMC algorithm.

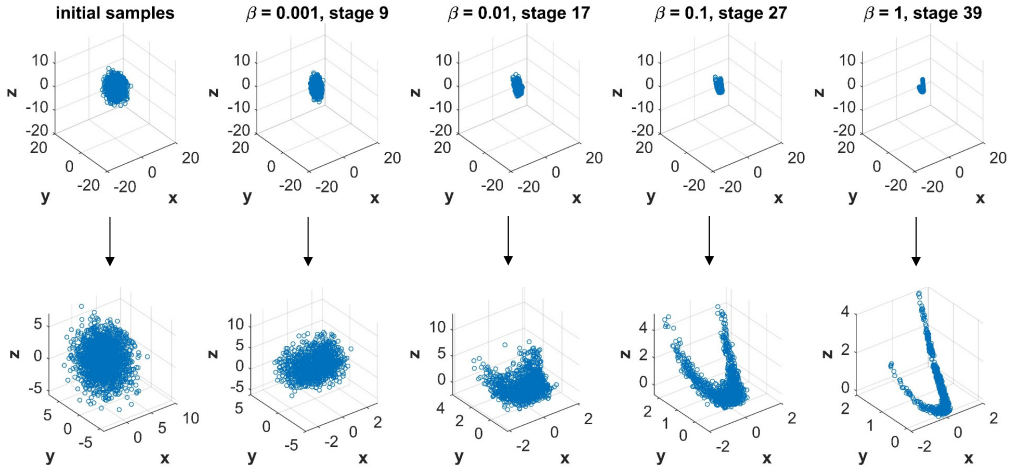
6. Inversion of Ultra-Deep Directional Resistivity Measurements

In this section, we investigate the performance of the GTMCMC algorithm and compare its results with those obtained from the standard TMCMC algorithm in the inversion of directional resistivity measurements. The inversion and interpretation of well-logging data play a crucial rule in real-time geosteering as it steers the well in a way that maximizes the contact with the pay zone [48]. Among several well-logging technologies, azimuthal resistivity logging-while-drilling (LWD) is widely used due to its relatively large depth of detection and azimuthal directional sensitivity [49]. The azimuthal resistivity well-logging data is challenging because the logging tool responses are usually nonlinear to formation topology. As the detection range of the logging tool grows, more parameters are needed to describe the underground formation of interest, which makes these inverse problems more challenging [50, 51].

Deterministic optimization methods such as Newton-based methods, are widely used in the industry [52, 51] due to their computational scalability. However, gradient-based approaches can only find local optima, with the result heavily depending on the initial guess. Even though one can apply multi-start methods [53] to increase the chances of finding the global optimal solution, deterministic optimization methods cannot provide associated uncertainty caused by noise in the data, which is integral to well-logging inverse problems. Therefore, stochastic methods based on Bayesian theory have drawn great attention in solving well-logging related problems in recent years. In Ref. [54] a decision-analytic framework to support high-quality geosteering decisions is implemented based on Bayesian inference. In Refs. [55] and [56] the authors proposed to use MCMC methods to obtain formation parameters of 1D earth models from synthetic directional resistivity well-logging data. Instead of inferring formation parameters of fixed dimensionality, the authors in [57, 58, 59] used trans-dimensional MCMC methods to infer parameters of earth models that can have a varied number of layers. Miao *et al.* [60] and Veettil *et al.* [61] proposed to infer well-bore locations from gamma-ray (GR) logging data using Bayesian approaches. In this work,



(a) TMCMC



(b) GTMCMC

Figure 6: 3D scatter plots of samples from different stages of the (a) TMCMC and (b) GTMCMC algorithms. The zoomed-in figures show the details of the sample distribution in different stages.

we solve the well-logging inverse problems using resistivity EM data with the GTMCMC algorithm, and compare its results with those obtained from the standard TMCMC method.

6.1. Ultra-Deep Directional Resistivity Measurements

The ultra-deep directional logging tool adopts multiple pairs of transmitter-receiver subs configured with different spacing and frequency. Figure 7 demonstrates a schematic diagram of a directional resistivity logging tool with 1 transmitter and 2 receivers. The tri-axial antennas are oriented at x-, y- and z-directions respectively. The working frequency can vary from one kHz to several hundreds kHz, thus enabling a large detection depth and a wide range of resistivity. Instead of directly using the tensor voltage, attenuation and phase shift signals delivered by the logging tool are used for model inversion [62].

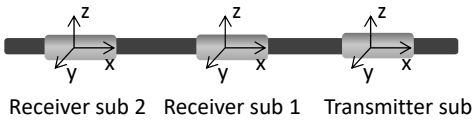


Figure 7: Schematic diagram of a directional EM LWD tool. The tool is configured with 1 transmitter and 2 receiver antennas.

In this work, we design a synthetic ultra-deep directional logging tool configured with 1 transmitter sub and 3 receiver subs. Three working frequencies, 2 kHz, 6 kHz and 24 kHz are available to three transmitter-receiver pairs. For each combination of spacing and frequency in a single channel, four types of phase shift and attenuation measurements are constructed based on the formation coupling tensors [63, 64]. The four types of measurements provide sensitivity to different geological features including the formation boundary, relative dip angle, bulk resistivity, and anisotropy respectively. As a result, 72 measurements are generated at each logging station, which corresponds to one unique set of model parameters. In total, there are 14400 measurements generated for 200 logging stations. We consider several noise levels for the phase shift (ps) and the attenuation signals (att). These are denoted as σ_{ps} and σ_{att} respectively.

6.2. Inversion of Ultra-Deep Directional Resistivity Measurements

The parameters of an 1D earth model are shown in Figure 8. Here, Rh_j represents the horizontal resistivity of the j-th layer, and DTB_j represents the distance from the LWD tool to the lower boundary of the j-th layer. A positive DTB value indicates that the boundary is below the logging tool

and vice versa, and $\mathrm{DTB}_i > \mathrm{DTB}_j$ if $i > j$. To make sure that the sampling algorithm always generates physically-meaningful DTB parameters, we transform DTB_j to thickness parameters $\mathrm{thk}_j > 0$ by

$$\mathrm{thk}_j = \mathrm{DTB}_j - \mathrm{DTB}_{j-1}, \quad j = 2, 3, ..., m-1 \tag{7}$$

As mentioned before, we also infer two noise standard deviations. Consequently, the inversion algorithm infers $(\mathrm{Rh}_1, \ldots, \mathrm{Rh}_m, \mathrm{DTB}_1, \mathrm{thk}_2, \ldots, \mathrm{thk}_{m-1}, \sigma_{ps}, \sigma_{att})$ for an m-layer 1D earth model. Considering the detection scope of the ultra-deep directional logging tool, the tested earth models have at most 7 layers in this investigation.

The LWD inverse problem can also be solved through pixel-based inversion [65, 66] that discretizes the underground formation into many thin layers so that one needs to infer only Rh for each thin layer to reconstruct the earth model. Pixel-based inversion offers more flexibility since it does not predetermine the number of layers, however, it involves dozens to hundreds of unknown parameters, which is impractical to be solved by a stochastic inverse algorithm in real-time. Therefore, we will focus on solving model-based LWD inverse problems in this paper.

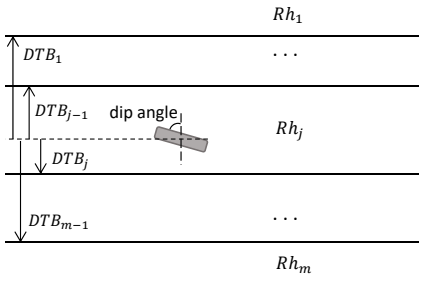


Figure 8: Parameters in an 1D earth model. The dip angle is considered to be known during the drilling process.

The inversion for the ultra-deep directional resistivity measurements requires numerous forward simulations, which is the most computationally intensive part in the inverse problem. TMCMC computes forward simulations for a set of samples independently in each stage, and it is therefore naturally parallelizable as opposed to most of the other MCMC methods. The model evaluations are performed in parallel via MPI [67] for efficient computations on a cluster with distributed computer cores [68].

6.3. Experimental Results

Given the subsurface structure is more or less similar at different logging points, we are able to incorporate information from the previous logging point into the current logging point with the GTMCMC algorithm. In this subsection, we show that the GTMCMC algorithm can improve the result of LWD inverse problems in a 2D earth model with much less computational cost, comparing to the standard TMCMC algorithm.

We test a 5-layer earth model shown in Figure 9. The ranges of model parameters are described in Table 2. The DTB parameters in the table is calculated assuming that the tool is located at 0 ft. As the tool moves forward, the true DTB parameters for each logging station changes based on the tool location. The standard deviations of noises added to the measurements are also treated as unknown parameters, with the true values $\sigma_{ps} = 0.75$ and $\sigma_{att} = 0.125$ for the phase-shift and the attenuation signals, respectively.

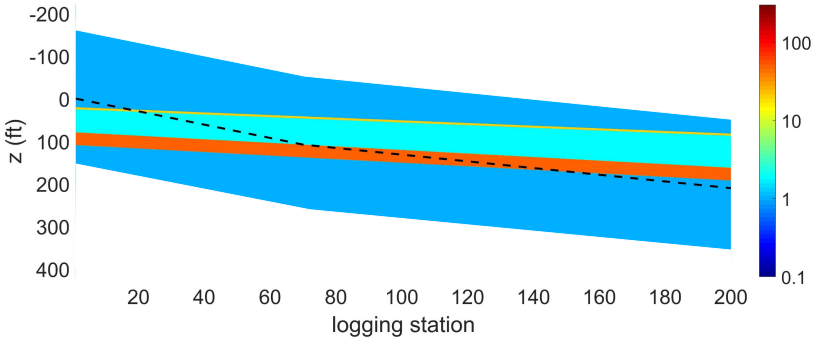


Figure 9: A 5-layer earth model. Measurements are taken at 200 logging stations along the drilling trajectory represented by the black dot line.

Table 2: True model parameters

Layer index	1	2	3	4	5
Rh ($\Omega \cdot m$)	1	20	2	50	1
DTB (ft)	20-82	25-87	79-162	109-192	-
thk (ft)	-	5	54-75	30	-

We employ weakly informative uniform distributions for the model parameters, with bounds shown in Table 3. For the GTMCMC algorithm, the

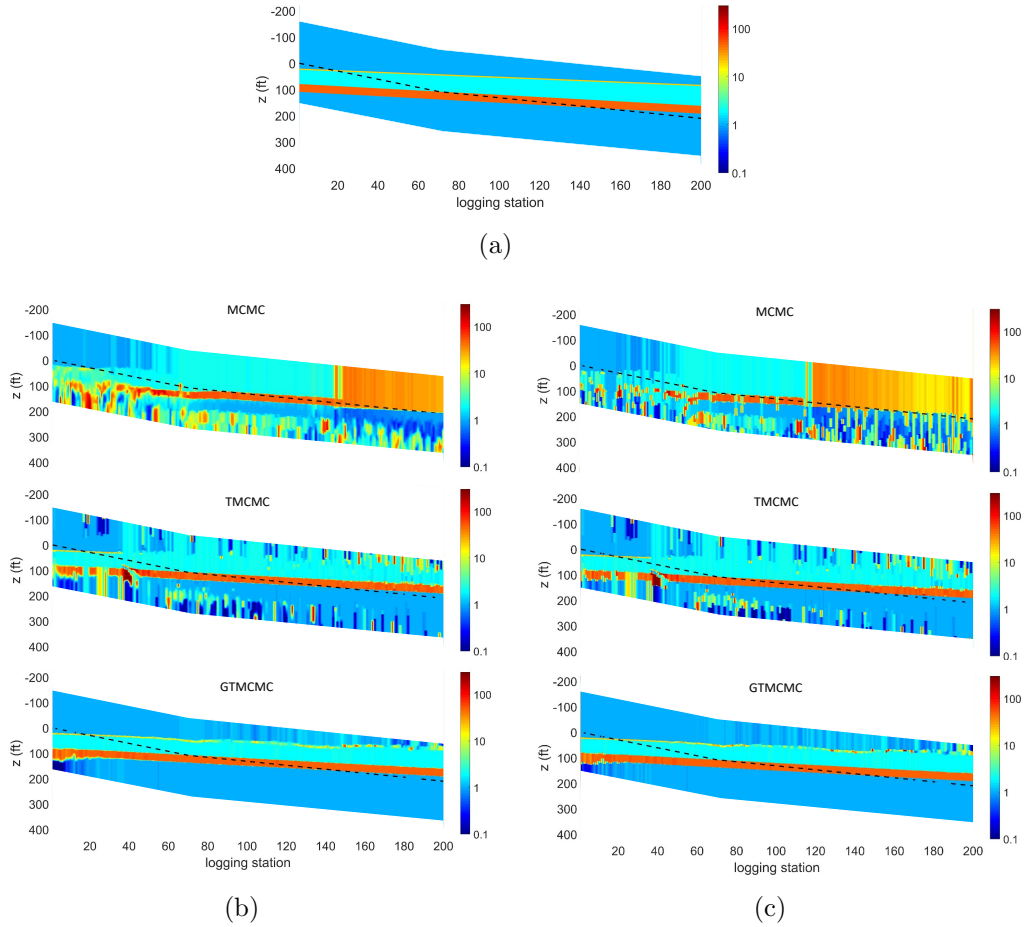
Table 3: Upper and lower boundaries of the uniform distribution

Parameter	$\ln(\sigma_{ps})$	$\ln(\sigma_{att})$	ln(Rh)	DTB_1	thk
min	-10	-10	-3	-200	5
max	10	10	3	200	100

importance distribution for the first logging point is equal to the prior distribution, since there is no information from a previous logging point. Starting from the second logging point, the importance distribution is a multi-variate Gaussian distribution with the mean vector and covariance matrix computed from samples of the previous logging point. The coefficient of variance CoV is set to 0.2 for all 1D inverse problems. We run the two algorithms on cluster with 200 Intel(R) Xeon(R) CPU E5-2650 v4 @2.20GHz CPUs with infiniBand interconnection, and 10^4 samples are generated at each TMCMC stage so that each CPU only handles computations for 50 samples. As a result, each inverse problem takes around 2 minutes to solve.

In addition to sampling the posterior distribution with TMCMC and GTMCMC, we also run adaptive Metropolis MCMC as the baseline. For a fair comparison, we set the number of samples for each algorithm differently so that the total number of forward evaluations of solving 200 problems are the same. As a result, the total number of forward evaluations are about 10^8, which is 5×10^5 for each problem in average. Note that to get physically meaningful mean results, we discretize the models before computing the mean results. The mean and MAP results of the three algorithms are compared with the true model in Figure 10. Given this sampling budget, the MCMC chains for high-dimensional LWD inverse problems are not converged. For all logging stations, only parameters of the closest layers can be inferred. The result from the TMCMC algorithm is more informative compared to the classical MCMC approach. With the same prior distribution at each logging station, the GTMCMC algorithm achieves better results than the TMCMC algorithm in the whole working range. Starting from logging station 40, the TMCMC algorithm starts to lose the identification of the top thin layer, which is only 5 ft thick. On the other hand, there exist sudden changes in the parameters between adjacent logging stations. For the GTMCMC algorithm, the initial samples are drawn from a importance distribution that is constructed with samples from the previous logging station, therefore, such sudden changes are limited. In addition, the GTMCMC algorithm can

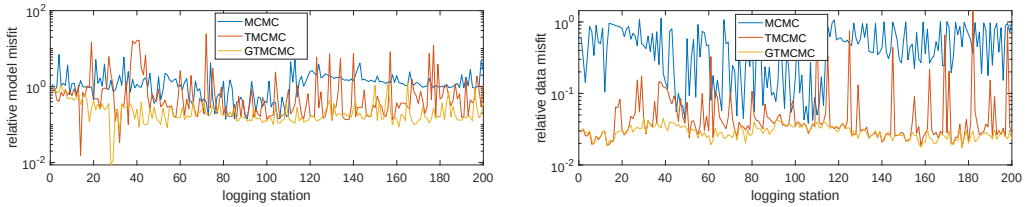
identify the top thin layer even though the logging tool is far from it. As a result, the 2D model resulted from the GTMCMC algorithm is smoother and visually more accurate than results generated by the MCMC and the TMCMC algorithms.



(a) (b) (c)

Figure 10: (a) The true model, (b) the mean prediction, and (c) the MAP prediction.

To evaluate the results obtained from the three sampling algorithms quantitatively, we calculate the parameter misfit and the model-data misfit of the mean models. In our experiments, the model parameters include resistivities and boundaries, so we convert the obtained models into pixel-based models to better calculate the parameter misfit. In the pixel-based model, the detection space is divided into 250 uniform thin layers so that the parameter



(a) (b)

Figure 11: Relative parameter (a) and data (b) misfits for the sampling algorithms tested in this section.

only includes 250 resistivities. The relative parameter misfit and relative model-data misfit are calculated as follows

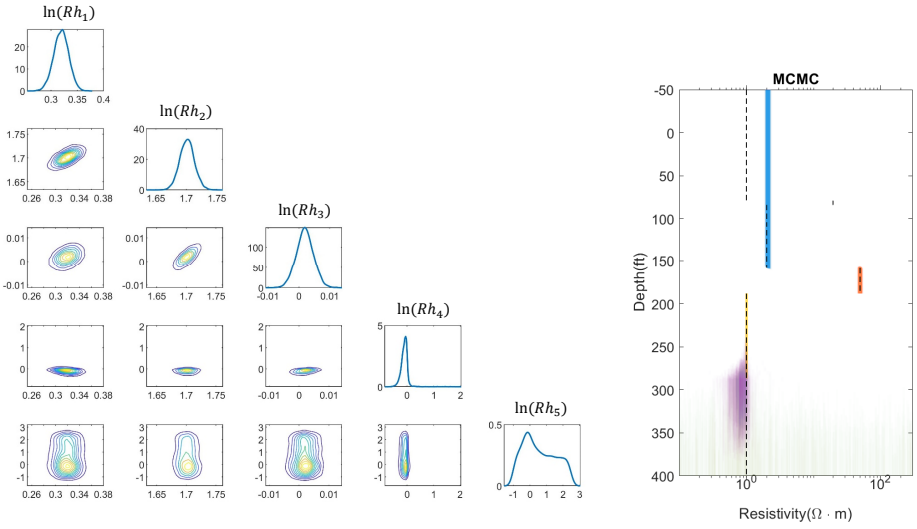
$$\text{relative parameter misfit} = \frac{\|\mathbf{m}_{\text{true}} - \mathbf{m}_{\text{inverse}}\|_2}{\|\mathbf{m}_{\text{true}}\|_2} \tag{8}$$

$$\text{relative data misfit} = \frac{\|\mathbf{d}_{\text{obs}} - \boldsymbol{f}(\mathbf{m}_{\text{inverse}})\|_2}{\|\mathbf{d}_{\text{obs}}\|_2} \tag{9}$$

with $\mathbf{m}_{\text{true}}$ the true model parameters, $\mathbf{m}_{\text{inverse}}$ the mean results from three sampling algorithms, $\mathbf{d}_{\text{obs}}$ the noised observation and $\boldsymbol{f}(\mathbf{m}_{\text{inverse}})$ the forward response of $\mathbf{m}_{\text{inverse}}$. We compute the relative model misfits and relative data misfits for 200 logging stations and shown them in Figure 11.

We examine results for logging station 190 as they are representative for the relative behavior of these models. Figures 12(a), 13(a), and 14(a) show the marginal posterior PDFs of the resistivity parameters in log scale. Figures 12(b), 13(b), and 14(b) show the image obtained by superimposing the values obtained for resistivity in the layered media when the tool is located at a depth of 200 ft. The vertical dot lines in the figures indicate the true resistivity of the layer. These results indicate different distributions of resistivities at logging station 190. From Figure 12(b) we can recognize 3 layers, which correspond to the bottom 3 layers in the ground truth model. However, the boundaries of the first 2 layers are missed. Figure 13(b) shows that 5 layers can be recognized from the TMCMC samples, however, only the last 3 layers match the ground truth model. From Figure 14(b) we recognize 5 layers, and the layer boundaries match the ground truth model well. The resistivities of the first two layers exhibit a higher uncertainty while the other three resistivities have very low uncertainty. These results

indicate that the use of importance distributions from related logging stations can help increase accuracy for the inferred model parameters with a given computational budget.

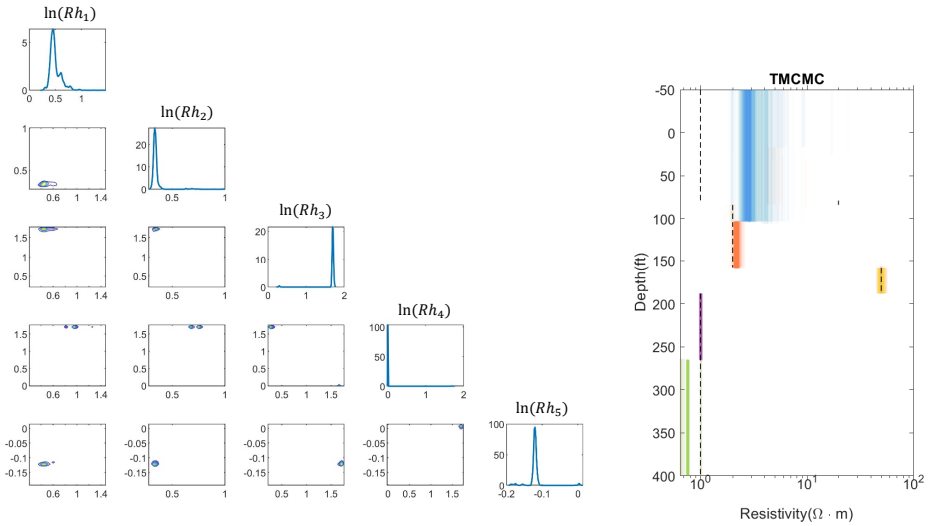


(a) Posterior PDFs of resistivities (b) Sample models

Figure 12: Statistics of the inversion result using MCMC at logging station 190. (a) Posterior PDFs of the resistivity parameters. (b) Image obtained by superimposing the values of resistivity in the layered media. The black dot line represents the ground truth.

7. Conclusions

Inspired by importance sampling, we presented a generalized transitional Markov chain Monte Carlo (GTMCMC) sampling strategy to improve the efficiency and generalize the applicability of TMCMC in tackling Bayesian inverse problems. With a judicious choice of importance PDF, GTMCMC is shown to reduce the otherwise prohibitive number of tempering stages when the prior PDF is significantly different from the target posterior. Furthermore, GTMCMC alleviates the challenge that TMCMC encounters when dealing with implicit priors as it no longer requires an initial set of samples from the prior PDF. Finally, the proposed generalization extends the applicability of TMCMC to inverse problems involving improper prior PDFs. Convergence analysis is provided in addition to numerical studies involving



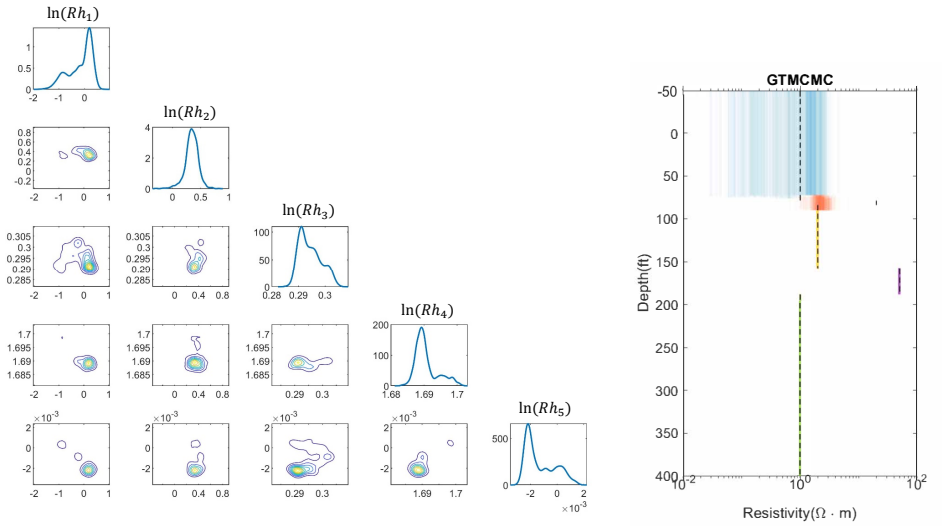
(a) Posterior PDFs of resistivities (b) Sample models

Figure 13: Statistics of the inversion result using TMCMC at logging station 190. (a) Posterior PDFs of the resistivity parameters. (b) Image obtained by superimposing the values of resistivity in the layered media. The black dot line represents the ground truth.

a variety of test problems, involving both Gaussian and non-Gaussian posterior PDFs, in which GTMCMC and TMCMC are compared and contrasted. The proposed GTMCMC algorithm was applied to a series of synthetic 1D logging-while-drilling inverse problems of relevance to the oil and gas industry, highlighting the enhanced efficiency and accuracy of GTMCMC over TMCMC and MCMC for such problems.

8. Acknowledgements

This material is based upon work supported by the U.S. Department of Energy, Office of Science, and Office of Advanced Science Computing Research, under Award Numbers DESC0017033. Sandia National Laboratories is a multimission laboratory managed and operated by National Technology and Engineering Solutions of Sandia, LLC, a wholly owned subsidiary of Honeywell International, Inc., for the U.S. Department of Energy's National Nuclear Security Administration under contract DE-NA0003525. This paper describes objective technical results and analysis. Any subjective views or opinions that might be expressed in the paper do not necessarily represent the



(a) Posterior PDFs of resistivities (b) Sample models

Figure 14: Statistics of the inversion result using GTMCMC at logging station 190. (a) Posterior PDFs of the resistivity parameters. (b) Image obtained by superimposing the values of resistivity in the layered media. The black dot line represents the ground truth.

views of the U.S. Department of Energy or the United States Government.

Appendix A. Proof Monotonically Decreasing KL-Divergence

Lemma 1. *Let the intermediate PDFs* $p_j(\theta)$ *and* $p_k(\theta)$ *be defined as in Equation* (5) *with annealing parameters* β_j *and* β_k *s.t.* $\beta_j > \beta_k$ *and* $\beta_j, \beta_k \in [0,1]$. *Further assume that* $D_{KL}[p(\theta \mid D) \mid\mid p_0(\theta)]$ *is finite. Then* $D_{KL}[p(\theta \mid D) \mid\mid p_j(\theta)] < D_{KL}[p(\theta \mid D) \mid\mid p_k(\theta)]$.

Proof. Let us define an arbitrary intermediate distribution as:

$$p_\beta(\theta) = \frac{\left(\frac{p(\theta|D)}{q(\theta)}\right)^\beta q(\theta)}{Z_\beta}. \tag{A.1}$$

Where the normalization is:

$$Z_\beta = \int \left(\frac{p(\theta \mid D)}{q(\theta)}\right)^\beta q(\theta)\, d\theta. \tag{A.2}$$

Then Lemma 1 $\Leftrightarrow \frac{\partial}{\partial\beta}\mathrm{D_{KL}}\left[p\left(\theta \mid D\right) \mid\mid p_\beta\left(\theta\right)\right] < 0$, i.e. monotonically decreasing in β, $\forall\beta \in [0,1]$.

$$\frac{\partial}{\partial\beta}\mathrm{D_{KL}}\left[p\left(\theta \mid D\right) \mid\mid p_\beta\left(\theta\right)\right] = \frac{\partial}{\partial\beta}\int p\left(\theta \mid D\right)\log\frac{p\left(\theta \mid D\right)}{p_\beta\left(\theta\right)}d\theta \tag{A.3}$$

$$= -\int p\left(\theta \mid D\right)\log\frac{p\left(\theta \mid D\right)}{Q\left(\theta\right)}d\theta + \int p_\beta\left(\theta\right)\log\frac{p\left(\theta \mid D\right)}{Q\left(\theta\right)}d\theta \tag{A.4}$$

$$= -\frac{1-\beta}{1-\beta}\left(\int p\left(\theta \mid D\right)\log\frac{p\left(\theta \mid D\right)}{Q\left(\theta\right)}d\theta - \int p_\beta\left(\theta\right)\log\frac{p\left(\theta \mid D\right)}{Q\left(\theta\right)}d\theta\right) \tag{A.5}$$

$$= \frac{-1}{1-\beta}\begin{pmatrix} \int p\left(\theta \mid D\right)\log\frac{p(\theta|D)}{Q(\theta)\left(\frac{p(\theta|D)}{Q(\theta)}\right)^\beta}d\theta + \log Z_\beta \\ -\int p_\beta\left(\theta\right)\log\frac{p(\theta|D)}{Q(\theta)\left(\frac{p(\theta|D)}{Q(\theta)}\right)^\beta}d\theta - \log Z_\beta \end{pmatrix} \tag{A.6}$$

$$= \frac{-1}{1-\beta}\left(\int p\left(\theta \mid D\right)\log\frac{p\left(\theta \mid D\right)}{p_\beta\left(\theta\right)}d\theta - \int p_\beta\left(\theta\right)\log\frac{p\left(\theta \mid D\right)}{p_\beta\left(\theta\right)}d\theta\right) \tag{A.7}$$

$$= \frac{-1}{1-\beta}\left(\mathrm{D_{KL}}\left[p\left(\theta \mid D\right) \mid\mid p_\beta\left(\theta\right)\right] + \mathrm{D_{KL}}\left[p_\beta\left(\theta\right) \mid\mid p\left(\theta \mid D\right)\right]\right) \tag{A.8}$$

$$\leq 0 \tag{A.9}$$

This follows because the KL divergence is always non-negative and $1-\beta$ is always non-negative for $\beta \in [0,1]$. This holds with equality only when $\mathrm{D_{KL}}\left[p_\beta\left(\theta\right) \mid\mid p\left(\theta \mid D\right)\right] = 0$ and $\mathrm{D_{KL}}\left[p_\beta\left(\theta\right) \mid\mid p\left(\theta \mid D\right)\right] = 0$ which occurs when $\beta = 1$ and $\mathrm{D_{KL}}\left[p\left(\theta \mid D\right) \mid\mid p_0\left(\theta\right)\right]$ is finite.

□

Lemma 1 means that the intermediate PDF $p_j\left(\theta\right)$ is closer to the posterior, $p\left(\theta \mid D\right)$, than $p_k\left(\theta\right)$ in terms of the informational theoretic Kullback-Leibler divergence. Since this holds for any pair β_j and β_k s.t. $\beta_j > \beta_k$ and $\beta_j, \beta_k \in [0,1]$, then we can conclude information is always being gained about the posterior through annealing. Of course for practical purposes, this assumes that the samples is adequately capturing the intermediate distribution which is asymptotically true as the number of samples grows.

Appendix B. Proof Monotonically Increasing CoV

Lemma 2. *Let the importance distribution $Q\left(\theta\right)$ be the initial distribution and the posterior $p\left(\theta \mid D\right)$ be the target distribution. Assume that $D_{KL}\left[p\left(\theta \mid D\right) \mid\mid Q\left(\theta\right)\right]$ is finite. Then $\forall\beta \in (0,1)$ the amount of information gained in the update*

from the initial distribution to the target distribution in the view of the intermediate distribution $p_\beta(\theta)$ is monotonically increasing in β.

Proof. The information gain from the initial distribution, $Q(\theta)$, to the target, $p(\theta \mid D)$ in the view of $p_\beta(\theta)$ is defined as:

$$\mathcal{I}_{p_\beta(\theta)}\left[p(\theta \mid D) \mid\mid Q(\theta)\right] = \int p_\beta(\theta) \log \frac{p(\theta \mid D)}{Q(\theta)} d\theta \tag{B.1}$$

Therefore,

$$\begin{aligned}
\frac{\partial}{\partial\beta}\mathcal{I}_{p_\beta(\theta)}\left[p(\theta \mid D) \mid\mid Q(\theta)\right] &= \frac{\partial}{\partial\beta}\int p_\beta(\theta) \log \frac{p(\theta \mid D)}{Q(\theta)} d\theta && \text{(B.2)}\\
&= \int p_\beta(\theta) \left(\log \frac{p(\theta \mid D)}{Q(\theta)}\right)^2 d\theta \\
&\quad - \left(\int p_\beta(\theta) \log \frac{p(\theta \mid D)}{Q(\theta)} d\theta\right)^2 && \text{(B.3)}\\
&\geq 0 && \text{(B.4)}
\end{aligned}$$

This inequality follows from Jensen's inequality. Thus $\mathcal{I}_{p_\beta(\theta)}\left[p(\theta \mid D) \mid\mid Q(\theta)\right]$ is monotonically increasing. Note that this line of reasoning holds also for a discrete random variable and where the integral is replaced by a sum. □

Lemma 3. *The coefficient of variation, κ, of sample weights defined by a change in β is monotonically increasing as β increases.*

Proof. The coefficient of variation is defined as:

$$\kappa = \frac{\sqrt{\int \left(\frac{p(\theta|D)}{Q(\theta)}\right)^{2\beta} Q(\theta)\, d\theta - \left(\int \left(\frac{p(\theta|D)}{Q(\theta)}\right)^{\beta} Q(\theta)\, d\theta\right)^2}}{\int \left(\frac{p(\theta|D)}{Q(\theta)}\right)^{\beta} Q(\theta)\, d\theta} \tag{B.5}$$

Therefore,

$$1 + \kappa^2 = \frac{\int \left(\frac{p(\theta|D)}{Q(\theta)}\right)^{2\beta} Q(\theta)\, d\theta}{\left(\int \left(\frac{p(\theta|D)}{Q(\theta)}\right)^{\beta} Q(\theta)\, d\theta\right)^2} \tag{B.6}$$

Differentiating with respect to β, we find:

$$\frac{\partial \kappa}{\partial \beta} = \frac{1+\kappa^2}{\kappa} \begin{pmatrix} \frac{\int \left(\frac{p(\theta|D)}{Q(\theta)}\right)^{2\beta} Q(\theta) \log \frac{p(\theta|D)}{Q(\theta)} d\theta}{\int \left(\frac{p(\theta|D)}{Q(\theta)}\right)^{2\beta} Q(\theta) d\theta} \\ -\frac{\int \left(\frac{p(\theta|D)}{Q(\theta)}\right)^{\beta} Q(\theta) \log \frac{p(\theta|D)}{Q(\theta)} d\theta}{\int \left(\frac{p(\theta|D)}{Q(\theta)}\right)^{\beta} Q(\theta) d\theta} \end{pmatrix} \tag{B.7}$$

$$= \frac{1+\kappa^2}{\kappa} \left(\int p_{2\beta}(\theta) \log \frac{p(\theta \mid D)}{Q(\theta)} d\theta - \int p_{\beta}(\theta) \log \frac{p(\theta \mid D)}{Q(\theta)} d\theta \right) \tag{B.8}$$

$$\geq 0 \tag{B.9}$$

This follows because κ is always positive and by the monotonic increase in information described by Lemma 2. Note that again we can follow a similar line of reasoning when considering the discrete estimation of the coefficient of variation where the mean and variance of the weights are estimated using samples and therefore the integrals are sums. Further, since the choice of $Q(\theta)$ is arbitrary, this holds of all stages of the algorithm. □

Because κ is monotonic then it can be easily optimized to a target level of variation using approaches like a bisector method.

References

[1] W. R. Gilks, S. Richardson, D. Spiegelhalter, Markov chain Monte Carlo in practice, Chapman and Hall/CRC, 1995.

[2] S. Brooks, A. Gelman, G. Jones, X.-L. Meng, Handbook of Markov chain Monte Carlo, CRC press, 2011.

[3] W. L. Dunn, J. K. Shultis, Exploring Monte Carlo methods, Elsevier, 2011.

[4] W. K. Hastings, Monte Carlo sampling methods using Markov chains and their applications, Oxford University Press, 1970.

[5] S.-K. Au, J. Beck, Important sampling in high dimensions, Structural safety 25 (2) (2003) 139–163.

[6] S. L. Cotter, G. O. Roberts, A. M. Stuart, D. White, MCMC methods for functions: modifying old algorithms to make them faster, Statistical Science (2013) 424–446.

[7] G. O. Roberts, J. S. Rosenthal, et al., Optimal scaling for various Metropolis-Hastings algorithms, Statistical science 16 (4) (2001) 351–367.

[8] C. P. Robert, V. Elvira, N. Tawn, C. Wu, Accelerating MCMC algorithms, WIREs Computational Statistics 10 (5) (2018) e1435.

[9] J. L. Beck, S.-K. Au, Bayesian updating of structural models and reliability using Markov chain Monte Carlo simulation, Journal of engineering mechanics 128 (4) (2002) 380–391.

[10] G. O. Roberts, J. S. Rosenthal, Examples of adaptive MCMC, Journal of Computational and Graphical Statistics 18 (2) (2009) 349–367.

[11] H. Haario, M. Laine, A. Mira, E. Saksman, DRAM: efficient adaptive MCMC, Statistics and computing 16 (4) (2006) 339–354.

[12] G. Desjardins, A. Courville, Y. Bengio, P. Vincent, O. Delalleau, Parallel tempering for training of restricted Boltzmann machines, in: Proceedings of the thirteenth international conference on artificial intelligence and statistics, MIT Press Cambridge, MA, 2010, pp. 145–152.

[13] S. Duane, A. D. Kennedy, B. J. Pendleton, D. Roweth, Hybrid Monte Carlo, Physics letters B 195 (2) (1987) 216–222.

[14] J. Ching, Y.-C. Chen, Transitional Markov chain Monte Carlo method for bayesian model updating, model class selection, and model averaging, Journal of engineering mechanics 133 (7) (2007) 816–832.

[15] P. Del Moral, A. Doucet, A. Jasra, Sequential Monte Carlo samplers, Journal of the Royal Statistical Society: Series B (Statistical Methodology) 68 (3) (2006) 411–436.

[16] N. Kantas, A. Beskos, A. Jasra, Sequential Monte Carlo methods for high-dimensional inverse problems: A case study for the Navier–Stokes equations, SIAM/ASA Journal on Uncertainty Quantification 2 (1) (2014) 464–489.

[17] A. Beskos, A. Jasra, N. Kantas, A. Thiery, et al., On the convergence of adaptive sequential Monte Carlo methods, Annals of Applied Probability 26 (2) (2016) 1111–1146.

[18] E. Marinari, G. Parisi, Simulated tempering: a new Monte Carlo scheme, EPL (Europhysics Letters) 19 (6) (1992) 451.

[19] G. A. Ortiz, D. A. Alvarez, D. Bedoya-Ruíz, Identification of Bouc–Wen type models using the transitional Markov chain Monte Carlo method, Computers & Structures 146 (2015) 252–269.

[20] W. Betz, I. Papaioannou, D. Straub, Transitional Markov chain Monte Carlo: observations and improvements, Journal of Engineering Mechanics 142 (5) (2016) 04016016.

[21] J. Ching, J.-S. Wang, Application of the transitional Markov chain Monte Carlo algorithm to probabilistic site characterization, Engineering Geology 203 (2016) 151–167.

[22] S.-H. Lee, J. Song, System identification of spatial distribution of structural parameters using modified transitional Markov chain Monte Carlo method, Journal of Engineering Mechanics 143 (9) (2017) 04017099.

[23] S. Wu, P. Angelikopoulos, C. Papadimitriou, P. Koumoutsakos, Bayesian annealed sequential importance sampling: an unbiased version of transitional Markov chain Monte Carlo, ASCE-ASME Journal of Risk and Uncertainty in Engineering Systems, Part B: Mechanical Engineering 4 (1).

[24] Y.-F. Jin, Z.-Y. Yin, W.-H. Zhou, S. Horpibulsuk, Identifying parameters of advanced soil models using an enhanced transitional Markov chain Monte Carlo method, Acta Geotechnica 14 (6) (2019) 1925–1947.

[25] T. A. Catanach, J. L. Beck, Bayesian updating and uncertainty quantification using sequential tempered mcmc with the rank-one modified metropolis algorithm, arXiv preprint arXiv:1804.08738.

[26] T. A. Catanach, H. D. Vo, B. Munsky, Bayesian inference of stochastic reaction networks using multifidelity sequential tempered Markov Chain Monte Carlo, International Journal for Uncertainty Quantification 10 (6).

[27] D. S. Ching, C. Safta, T. A. Reichardt, Sensitivity-Informed Bayesian Inference for Home PLC Network Models with Unknown Parameters, Energies 14 (9). doi:10.3390/en14092402.

[28] R. H. Swendsen, J.-S. Wang, Replica Monte Carlo simulation of spin-glasses, Physical review letters 57 (21) (1986) 2607.

[29] C. J. Geyer, Markov chain Monte Carlo maximum likelihood, Interface Foundation of North America, 1991.

[30] D. J. Earl, M. W. Deem, Parallel tempering: Theory, applications, and new perspectives, Physical Chemistry Chemical Physics 7 (23) (2005) 3910–3916.

[31] D. Sivia, J. Skilling, Data analysis: a Bayesian tutorial, Oxford University Press, 2006.

[32] P. Bisaillon, R. Sandhu, M. Khalil, C. Pettit, D. Poirel, A. Sarkar, Bayesian parameter estimation and model selection for strongly nonlinear dynamical systems, Nonlinear Dynamics 82 (3) (2015) 1061–1080.

[33] R. Sandhu, C. Pettit, M. Khalil, D. Poirel, A. Sarkar, Bayesian model selection using automatic relevance determination for nonlinear dynamical systems, Computer Methods in Applied Mechanics and Engineering 320 (2017) 237–260.

[34] J. A. Hoeting, D. Madigan, A. E. Raftery, C. T. Volinsky, Bayesian model averaging: a tutorial, Statistical science (1999) 382–401.

[35] L. Wasserman, Bayesian model selection and model averaging, Journal of mathematical psychology 44 (1) (2000) 92–107.

[36] S. Asmussen, P. W. Glynn, Stochastic simulation: algorithms and analysis, Vol. 57, Springer Science & Business Media, 2007.

[37] P. Green, Bayesian system identification of dynamical systems using large sets of training data: A MCMC solution, Probabilistic Engineering Mechanics 42 (2015) 54–63.

[38] P. L. Green, Bayesian system identification of a nonlinear dynamical system using a novel variant of simulated annealing, Mechanical Systems and Signal Processing 52 (2015) 133–146.

[39] P. Angelikopoulos, C. Papadimitriou, P. Koumoutsakos, X-TMCMC: Adaptive kriging for Bayesian inverse modeling, Computer Methods in Applied Mechanics and Engineering 289 (2015) 409–428.

[40] A. Gelman, J. B. Carlin, H. S. Stern, D. B. Dunson, A. Vehtari, D. B. Rubin, Bayesian data analysis, CRC press, 2013.

[41] J. Baxter, A Bayesian/information theoretic model of learning to learn via multiple task sampling, Machine learning 28 (1) (1997) 7–39.

[42] A. M. Stuart, Inverse problems: a Bayesian perspective, Acta numerica 19 (2010) 451–559.

[43] J. S. Rosenthal, et al., Optimal proposal distributions and adaptive MCMC, Handbook of Markov Chain Monte Carlo 4 (10.1201).

[44] T. A. Catanach, Computational methods for Bayesian inference in complex systems, Ph.D. thesis, California Institute of Technology (2017).

[45] R. M. Neal, Probabilistic inference using Markov chain Monte Carlo methods, Department of Computer Science, University of Toronto Toronto, Ontario, Canada, 1993.

[46] G. Fishman, Monte Carlo: concepts, algorithms, and applications, Springer Science & Business Media, 2013.

[47] R. M. Neal, Annealed importance sampling, Statistics and computing 11 (2) (2001) 125–139.

[48] W. Lesso Jr, S. Kashikar, et al., The principles and procedures of geosteering, in: SPE/IADC Drilling Conference, Society of Petroleum Engineers, 1996.

[49] M. S. Bittar, Electromagnetic wave resistivity tool having a tilted antenna for determining the horizontal and vertical resistivities and relative dip angle in anisotropic earth formations, uS Patent 6,163,155 (Dec. 19 2000).

[50] K. Key, 1D inversion of multicomponent, multifrequency marine CSEM data: Methodology and synthetic studies for resolving thin resistive layers, Geophysics 74 (2) (2009) F9–F20.

[51] R. Beer, L. C. T. Dias, A. M. V. da Cunha, M. R. Coutinho, G. H. Schmitt, J. Seydoux, C. Morriss, E. Legendre, J. Yang, Q. Li,

et al., Geosteering and/or reservoir characterization the prowess of new-generation LWD tools, in: SPWLA 51st Annual Logging Symposium, Society of Petrophysicists and Well-Log Analysts, 2010.

[52] T. M. Habashy, A. Abubakar, A general framework for constraint minimization for the inversion of electromagnetic measurements, Progress in electromagnetics Research 46 (2004) 265–312.

[53] R. Martí, Multi-start methods, in: Handbook of metaheuristics, Springer, 2003, pp. 355–368.

[54] K. Kullawan, R. Bratvold, J. E. Bickel, et al., A decision analytic approach to geosteering operations, SPE Drilling & Completion 29 (01) (2014) 36–46.

[55] Q. Shen, X. Wu, J. Chen, Z. Han, Y. Huang, Solving geosteering inverse problems by stochastic hybrid Monte Carlo method, Journal of Petroleum Science and Engineering 161 (2018) 9–16.

[56] H. Lu, Q. Shen, J. Chen, X. Wu, X. Fu, Parallel multiple-chain DRAM MCMC for large-scale geosteering inversion and uncertainty quantification, Journal of Petroleum Science and Engineering 174 (2019) 189–200.

[57] B. J. Minsley, A trans-dimensional Bayesian Markov chain Monte Carlo algorithm for model assessment using frequency-domain electromagnetic data, Geophysical Journal International 187 (1) (2011) 252–272.

[58] M. Sambridge, T. Bodin, K. Gallagher, H. Tkalčić, Transdimensional inference in the geosciences, Philosophical Transactions of the Royal Society A: Mathematical, Physical and Engineering Sciences 371 (1984) (2013) 20110547.

[59] Q. Shen, J. Chen, X. Wu, Z. Han, Y. Huang, Parallel tempered trans-dimensional Bayesian inference for the inversion of ultra-deep directional logging-while-drilling resistivity measurements, Journal of Petroleum Science and Engineering 188 (2020) 106961.

[60] Y. Miao, D. R. Kowal, N. Panchal, J. Vila, M. Vannucci, Nonlinear state-space modeling approaches to real-time autonomous geosteering, Journal of Petroleum Science and Engineering 189 (2020) 107025.

[61] D. R. A. Veettil, K. Clark, et al., Bayesian geosteering using sequential Monte Carlo methods, Petrophysics 61 (01) (2020) 99–111.

[62] J. Seydoux, E. Legendre, E. Mirto, C. Dupuis, J.-M. Denichou, N. Bennett, G. Kutiev, M. Kuchenbecker, C. Morriss, L. Yang, et al., Full 3d deep directional resistivity measurements optimize well placement and provide reservoir-scale imaging while drilling, in: SPWLA 55th annual logging symposium, Society of Petrophysicists and Well-Log Analysts, 2014.

[63] Q. Li, D. Omeragic, L. Chou, L. Yang, K. Duong, et al., New directional electromagnetic tool for proactive geosteering and accurate formation evaluation while drilling, in: SPWLA 46th annual logging symposium, Society of Petrophysicists and Well-Log Analysts, 2005.

[64] C. Dong, C. Dupuis, C. Morriss, E. Legendre, E. Mirto, G. Kutiev, J.-M. Denichou, M. Viandante, J. Seydoux, N. Bennett, et al., Application of automatic stochastic inversion for multilayer reservoir mapping while drilling measurements, in: Abu Dhabi International Petroleum Exhibition and Conference, Society of Petroleum Engineers, 2015.

[65] Y. Lin, A. Abubakar, T. Habashy, G. Pan, M. Li, V. Druskin, L. Knizhnerman, Schemes for improving efficiency of pixel-based inversion algorithms for electromagnetic logging-while-drilling measurements, in: SEG Technical Program Expanded Abstracts 2012, Society of Exploration Geophysicists, 2012, pp. 1–5.

[66] M. Thiel, D. Omeragic, High-fidelity real-time imaging with electromagnetic logging-while-drilling measurements, IEEE Transactions on Computational Imaging 3 (2) (2017) 369–378.

[67] W. Gropp, W. D. Gropp, E. Lusk, A. D. F. E. E. Lusk, A. Skjellum, Using MPI: portable parallel programming with the message-passing interface, Vol. 1, MIT press, 1999.

[68] C. Safta, M. Khalil, H. N. Najm, Transitional Markov chain Monte Carlo sampler in UQTk, Tech. Rep. SAND2020-3166, Sandia National Lab.(SNL-CA), Livermore, CA (United States) (2020).